Lymphatic Metastasis in the Absence of Functional Intratumor Lymphatics

Timothy P. Padera,[1] Ananth Kadambi,[1]* Emmanuelle di Tomaso,[1] Carla Mouta Carreira,[1]† Edward B. Brown,[1] Yves Boucher,[1] Noah C. Choi,[1] Douglas Mathisen,[2] John Wain,[2] Eugene J. Mark,[3] Lance L. Munn,[1] Rakesh K. Jain[1]‡

Lymphatic metastasis contributes to mortality from solid tumors. Whether metastasizing cancer cells reach lymph nodes via intratumor lymphatic vessels is unknown. Here, we examine functional lymphatics associated with mouse tumors expressing normal or elevated levels of vascular endothelial growth factor–C (VEGF-C), a molecule that stimulates lymphangiogenesis. Although VEGF-C overexpression increased lymphatic surface area in the tumor margin and lymphatic metastasis, these tumors contained no functional lymphatics, as assessed by four independent functional assays and immunohistochemical staining. These findings suggest that the functional lymphatics in the tumor margin alone are sufficient for lymphatic metastasis and should be targeted therapeutically.

Cancer cells metastasize to distant sites via the vascular or lymphatic system. Our insight into the lymphatic system lags far behind that of the vascular system, due largely to the limitations of available techniques. To date, studies investigating lymphatics in tumors have relied exclusively on either molecular markers (*1*, *2*) or functional techniques (*3*–*5*). The former studies have identified lymphatic markers in tumors, whereas the latter have failed to demonstrate functional intratumor lymphatics (*1*, *2*, *4*). Functional lymphatics, however, do exist in the tumor margin (defined as <100 μm from the tumor edge) (*5*). These disparate observations call into question the relation between functional lymphatic vessels and widely accepted lymphatic molecular markers and the role they play in lymphatic metastasis.

To address these issues, we created two stable cell lines from T-241 murine fibrosarcoma and B16-F10 murine melanoma that overexpress vascular endothelial growth factor–C (VEGF-C), a known lymphangiogenic molecule (*6*, *7*) (fig. S1A). We implanted both mock-transduced and VEGF-C–overexpressing tumor lines orthotopically in the hindlimb of nude mice (*8*) (see supplementary Materials and Methods) (fig. S1B). VEGF-C–overexpressing melanomas and fibrosarcomas exhibited an increase in lymphatic metastasis (fig. S1C) but no increase in hematogenous lung metastasis (Table 1). VEGF-C–overexpressing melanomas also showed increased local invasion (Table 1). VEGF-C, however, did not significantly alter migration of either cell line in vitro (fig. S1D).

To determine whether intratumor lymphatics were present, we stained both tumor types for the putative lymphatic markers LYVE-1 (*9*) and Prox 1 (*10*), along with the murine pan-endothelial marker MECA-32 (*11*–*13*) (Fig. 1, A to C). VEGF-C–overexpressing tumors exhibited more extensive LYVE-1 and MECA-32 staining, as compared to mock-transduced tumors (Fig. 1D), especially in the tumor margin (Fig. 1E). Morphologically, LYVE-1–positive structures in the tumor appeared to be vessels that had collapsed or become filled with tumor cells that occlude the lumen, with very few structures having an open lumen (Fig. 1F). In contrast, LYVE-1–positive structures exhibited a more normal lymphatic morphology in the tumor margin.

Surprisingly, ~10% of all tumor-associated LYVE-1–positive structures either colocalized with the intravenous lectin, a marker of perfused blood vessels, or contained red blood cells (fig. S2, A and B; table S1). This strongly suggests that a fraction of LYVE-1–stained structures in our B16-F10 melanoma and T-241 fibrosarcoma models are blood vessels. In the dermis of normal tail, however, LYVE-1–positive structures did not colocalize with lectin-perfused blood vessels. Inside both tumor types, there was an ~50% decrease in colocalization of MECA-32 (*14*) or Prox 1 (see supplementary Materials and Methods) with LYVE-1–positive structures when compared to normal tissue and the tumor margin (table S1).

To correlate structure with function, we performed four functional assays. We measured interstitial fluid pressure (IFP) in VEGF-C–overexpressing and control T-241 fibrosarcomas and found no difference, although the tumors exhibited higher IFP than did normal tail tissue (Fig. 2A). The universal finding that tumors have elevated IFP suggests that tumors lack functional lymphatics (*15*). IFP, however, like molecular clearance rate (*16*), depends on many parameters other than lymphatic function, including blood vessel permeability, microvascular pressure, and tissue hydraulic conductivity (*15*, *17*). Thus, to analyze functional lymphatics directly, we performed three different microlymphangiography assays. Lymphangiography involves injecting labeled macromolecules into the interstitium for uptake into lymphatics and provides microscopic demarcation of functional draining lymphatics, as demonstrated in normal tail (Fig. 2B) (*18*).

Multiphoton laser-scanning microscopy (MPLSM) allowed three-dimensional, high-resolution imaging of blood and lymphatic vessels at depths extending 400 μm below the surface of the skin (*18*, *19*) (Fig. 2, C and

Table 1. Invasion and metastasis from mock-transduced (MT) and VEGF-C–overexpressing tumors. The numerator is the number of mice that exhibited the property, and the denominator is the total number of mice.

Property	Cell line		*P* value*
	B16F10-MT	*B16F10-VEGF-C*	
Lymphatic metastasis	6/21	15/19	0.002
Local invasion	3/21	12/18	0.001
Lung metastasis†	5/22	2/19	NS
	T-241-MT	*T-241-VEGF-C*	
Lymphatic metastasis	2/14	8/14	0.046
Local invasion	4/14	5/14	NS
Lung metastasis†	5/14	6/14	NS

*P value based on Fisher's exact test. NS, not significant. †Hematogenous metastasis was analyzed microscopically in 10 to 20 sections of lung per animal.

[1]E. L. Steele Laboratory, Department of Radiation Oncology, [2]Department of Surgery, [3]Department of Pathology, Massachusetts General Hospital, Harvard Medical School, 100 Blossom Street, Boston, MA 02114, USA.

*Present address: Comprehensive Cancer Center, University of California-San Francisco, 2340 Sutter Street, N461, San Francisco, CA 94143-0808, USA.
†Present address: Center for Molecular Medicine, Maine Medical Center Research Institute, 81 Research Drive, Scarborough, ME 04074, USA.
‡To whom correspondence should be addressed. E-mail: jain@steele.mgh.harvard.edu

D). VEGF-C increased the diameter of functional lymphatics in the tumor margin by 26%, as compared to mock-transduced controls (Fig. 2E) (*20*), in a tumor size–independent manner ($p > 0.05$). No intratumor lymphatics were observed more than 260 μm below the surface of the skin (*21*), in accord with our previous report (*5*). Blood vessels were clearly visible at these depths using MPLSM. VEGF-C overexpression did not induce functional intratumoral lymphatic vessels. The virtual absence of lymphatic function between 100 and 400 μm into these fibrosarcomas indicates that any deeper structures would not connect to the functional lymphatic network outside the tumor.

Next, using epifluorescence microscopy, we discerned the architecture of the functional lymphatic network in the tumor margin of T-241 fibrosarcomas. Strikingly, superficial lymphatics maintained the approximate hexagonal pattern observed in normal dermis (Fig. 2, B and F), suggesting that they were preexisting lymphatic vessels of the normal tissue overlying the tumor. However, tumor VEGF-C overexpression increased the diameter of lymphatics in the tumor margin (Fig. 2G), which is consistent with the MPLSM results (Fig. 2E) and studies of VEGF-C overexpression in the skin (*22*).

Last, we performed ferritin microlymphangiography (*5*) to probe deeper than 400 μm into the tumor and subsequently stained for LYVE-1, Prox 1, MECA-32, and intravenous lectin (Fig. 1, A to C). Given that only lymphatics near the injection site and subsequent drainage areas can be identified by this method, we focused our experiments on detecting potential intratumor lymphatics by injecting deeply into the tumor. Ferritin staining in VEGF-C–overexpressing and mock-transduced tumors did not colocalize with LYVE-1 in any of the 14 fibrosarcomas stained, again suggesting that LYVE-1–positive structures within these tumors are not functional lymphatics (table S1 and fig. S3A). In contrast, ~85% of ferritin staining colocalized with LYVE-1 and MECA-32 in both the tumor margin and normal tissue, confirming that lymphatics in these areas are functional. Ferritin in the tumor appeared to travel through nonendothelialized channels and accumulated in the skin, distant from the injection site, where it was absorbed by functional tumor margin lymphatics (fig. S3B). This was also observed in MPLSM experiments. Taken together, these data suggest the following: (i) intratumor transport of injected contrast agent does not occur through lymphatic vessels, but rather through preferential pathways in the interstitium lacking endothelial lining (*4*); and (ii) LYVE-1 alone cannot be used to detect functional lymphatics.

We also performed ferritin lymphangiography and immunohistochemistry on five tumors (four adenocarcinomas and one fibrosarcoma) arising spontaneously in aged C3H/Sed mice for comparison with our results from tumor xenografts. In these tumors, the density of LYVE-1 staining was 5.2 ± 2.8 structures per mm^2 and the functional vascular density was 317 ± 107 structures per mm^2, based on lectin staining. The tumors consisted of multiple lobules separated by large connective tissue tracts containing vessels. LYVE-1 staining was commonly observed in the connective tissue tracts inside the tumor, but these structures did not take up ferritin after intratumor microlymphangiography (Fig. 3, A and B). The IFP in these tumors was elevated (10.5 ± 1.7 mm Hg), corroborating the lack of functional lymphatic drainage from the tumor, as determined by ferritin microlymphangiography.

Finally, we measured IFP in lung tumors in patients before surgical resection and stained these tumors for LYVE-1, Prox 1, and CD31. Ten of these 22 patients (10 with adenocarcinomas, 8 with squamous cell carcinomas, 3 with bronchioloalveolar carcinomas, and 1 with small cell carcinoma) had lymph node metastasis. The average postsurgical survival was 4.4 ± 0.7 years (table S2). Tumor IFP in these patients was elevated (9.5 ± 1.6 mm Hg). There was no correlation between IFP and lymph node metastasis (fig. S4A), in contrast to a recent animal study (*23*). Only five tumors exhibited LYVE-1–positive structures in the tumor margin (defined as ~500 μm from the tumor edge, because of difficulties in exactly identifying the tumor edge), and none exhibited staining in the bulk of the tumor. Additionally, in a few cases, LYVE-1 marked capillaries in the alveolar walls, which do not possess lymphatics, as well as endothelial cells of an occasional artery and vein, confounding the interpretation of this stain (fig. S4B). CD31, however, showed preservation of alveolar capillaries deep within these tumors, particularly those with bronchioloalveolar growth patterns (fig. S4C). There was no correlation between LYVE-1 staining and IFP, lymph node metastasis, or overall survival in these patients (see supplementary Materials and Methods). These data suggest that human lung tumors do not contain functional lym-

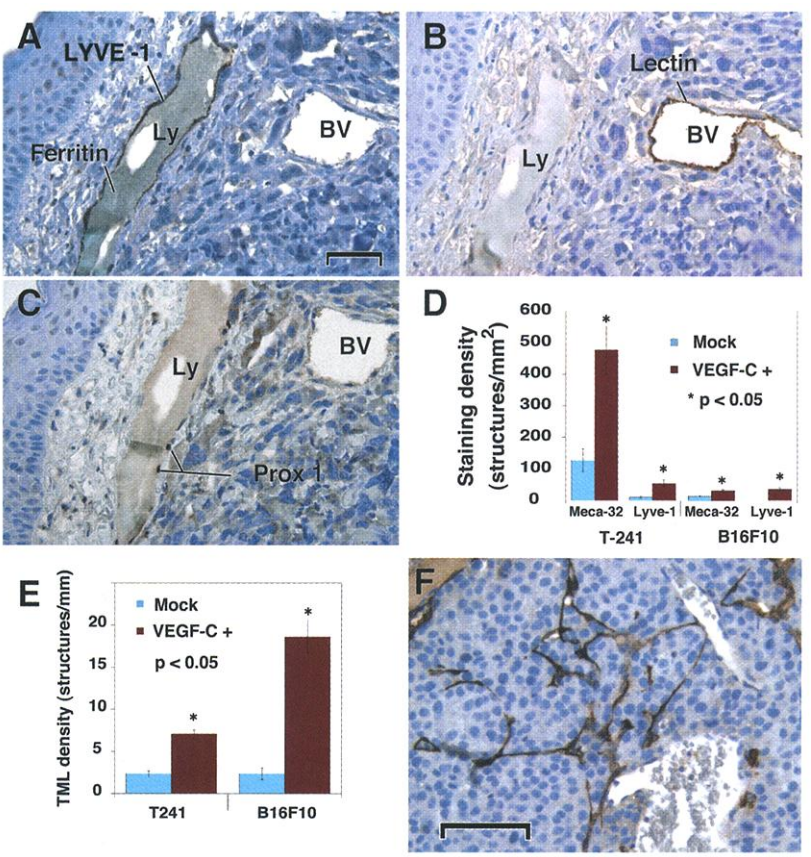

Fig. 1. Immunohistochemical characterization of lymphatic markers. (**A**) LYVE-1 stain (brown) of a ferritin-filled lymphatic vessel (Ly) at the edge of a T-241 fibrosarcoma. (**B**) Lectin stain (brown) showing a neighboring blood vessel (BV). (**C**) Prox 1 stain (nuclear, brown) of same lymphatic vessel. (**D**) VEGF-C–overexpressing tumors exhibited higher staining densities, as compared to control tumors. (**E**) VEGF-C–overexpressing tumors exhibited higher LYVE-1–staining densities in tumor margin (referred to as TML), as compared to MT tumors. (**F**) Structures stained with LYVE-1 (brown) were compressed or filled with cancer cells in B16-F10 melanoma. Error bars show SEM. Scale bars: (A), (B), (C), and (F), 100 μm.

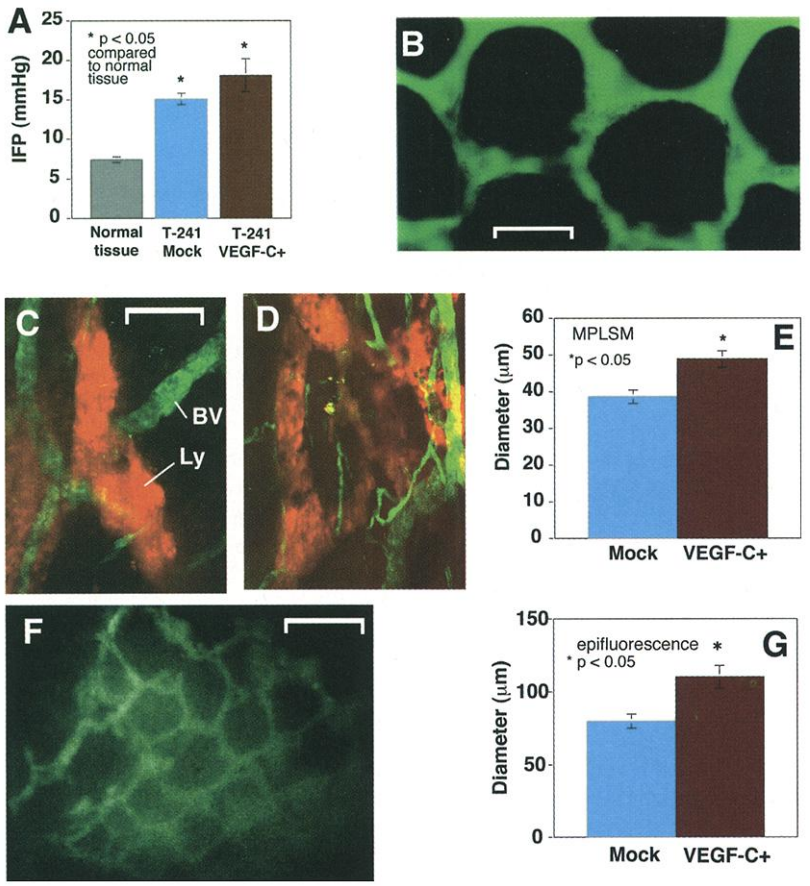

Fig. 2. Evaluation of tumor lymphatic function. (**A**) IFP was elevated in T-241 fibrosarcoma tissue, as compared to in normal tail, but VEGF-C overexpression did not alter IFP. (**B**) Epifluorescence lymphangiography of normal tail showing a hexagonal pattern of lymphatic network. (**C** and **D**) Maximum intensity projection of MPLSM images from combined angiography and lymphangiography in T-241 fibrosarcoma. Functional lymphatics (red, Ly) and nearby blood vessels (green, BV) are shown at the tumor margin. (**E**) Functional tumor margin lymphatics (TMLs) in VEGF-C–overexpressing T-241 fibrosarcomas have larger diameters, as compared to those in control tumors, as determined by MPLSM. (**F**) Epifluorescence lymphangiography showing functional lymphatic vessels in the margin of T-241 fibrosarcoma with a distorted, yet somewhat normal, hexagonal network, suggesting that they are preexisting vessels, not newly formed. (**G**) Functional TMLs in VEGF-C–overexpressing T-241 fibrosarcomas have larger diameters, as compared to control tumors, as determined by epifluorescence microscopy. Error bars show SEM. Scale bars: (B), 250 μm; (C) and (D), 100 μm; (F), 500 μm.

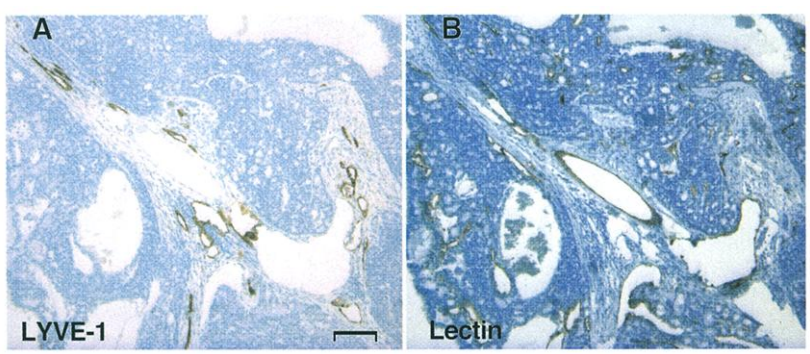

Fig. 3. Evaluation of spontaneous tumors arising in aging mice. (**A**) LYVE-1 stain of tumor showing LYVE-1–positive structures in fibrous tissue between tumor lobule with no LYVE-1 stain within the tumor lobule. No colocalization with intratumorally injected ferritin was seen in any similar structures, suggesting that these structures do not collect fluid or macromolecules from the tumor lobules. (**B**) Adjacent section stained for lectin, showing perfusion of both the tumor lobules as well as the interlobular connective tissue. There was no colocalization of lectin and LYVE-1 seen in this section. Scale bar, 300 μm.

phatics and that LYVE-1 staining is not clinically predictive in this setting.

The mechanisms underlying the lack of lymphatic function in tumors are not understood. The following are possible: (i) the primary valve structure (*24*) is lacking in the LYVE-1–positive structures in tumors, preventing effective fluid uptake and lymphatic function; (ii) the mechanical forces generated by the growing tumor cells collapse lymphatics, rendering them nonfunctional (*25*); or (iii) invading tumor cells destroy the lymphatic network, leaving only remnant endothelia inside the tumor.

Regardless of the etiology for the lack of functional lymphatics in tumors, we propose that functional lymphatics in the tumor margin are sufficient for lymphatic metastasis, because (i) increases in lymphatic surface area (and thus more opportunity for cancer cell intravasation) were accompanied by increases in lymphatic metastasis in VEGF-C–overexpressing tumors (Fig. 2E and Table 1) (*26*), and (ii) tumors that lack intratumor LYVE-1 staining still metastasize (table S2) (*26*). The increase in LYVE-1 staining in VEGF-C–overexpressing tumors (Fig. 1, D and E) (*16*, *27*, *28*) suggests that VEGF-C may act as a survival factor (*29*) for the endothelial cells of lymphatic vessels compressed or destroyed by the growing tumor (*3–5*, *25*) (Fig. 1F) and as a mitogen for lymphatic endothelial cells in the tumor margin (see supplementary Materials and Methods). The ability of VEGF-C to (i) serve as a survival factor for lymphatic endothelial cells, (ii) induce lymphatic metastases by increasing the functional lymphatic surface area in the tumor margin, and (iii) induce angiogenesis in some tumors (*7*, *16*), makes VEGF-C an ideal target for controlling both tumor growth and metastasis.

Note added in proof: LYVE-1/Prox 1–positive structures in two human breast cancer cell lines (MDA-231 and MDA-435S) grown orthotopically in mice also did not colocalize with a functional lymphatic marker (ferritin) within the tumor; however, they did so in the tumor margin, consistent with the findings of this report (*30*).

References and Notes

1. M. S. Pepper, *Clin. Cancer Res.* **7**, 462 (2001).
2. R. K. Jain, B. T. Fenton, *J. Natl. Cancer Inst.* **94**, 417 (2002).
3. F. C. Lee, R. C. Tilghman, *Arch. Surg.* **26**, 602 (1933).
4. P. M. Gullino, in *Biological Responses to Cancer*, E. Mihich, Ed. (Plenum Press, New York, 1985), vol. 4, pp. 1–20.
5. A. J. Leu, D. A. Berk, A. Lymboussaki, K. Alitalo, R. K. Jain, *Cancer Res.* **60**, 4324 (2000).
6. T. Karpanen, K. Alitalo, *J. Exp. Med.* **194**, F37 (2001).
7. A. Kadambi *et al.*, *Cancer Res.* **61**, 2404 (2001).
8. T. Todoroki, H. D. Suit, *J. Surg. Oncol.* **29**, 207 (1985).
9. D. G. Jackson, R. Prevo, S. Clasper, S. Banerji, *Trends Immunol.* **22**, 317 (2001).
10. J. T. Wigle, G. Oliver, *Cell* **98**, 769 (1999).
11. C. Mouta Carreira *et al.*, *Cancer Res.* **61**, 8079 (2001).

12. J. P. Sleeman, J. Krishnan, V. Kirkin, P. Baumann, *Microsc. Res. Tech.* **55**, 61 (2001).
13. Lymphatic vessels were classified as follows: normal tissue lymphatics (NTL); tumor margin lymphatics (TML), found within 150 μm of the surface of skin overlying the tumor; and intratumor lymphatics (ITL), found farther than 150 μm from the surface of the overlying the tumor. The 150-μm delineation comes from the addition of ~50 μm for the thickness of the skin and 100 μm, designated as the tumor margin in previous studies (*5*).
14. MECA-32 may not stain 100% of vascular and lymphatic endothelium.
15. R. K. Jain, *Sci. Am.* **271**, 58 (July 1994).
16. M. Skobe *et al.*, *Am. J. Pathol.* **159**, 893 (2001).
17. G. W. Schmid-Schonbein, *Physiol. Rev.* **70**, 987 (1990).
18. T. P. Padera, B. S. Stoll, P. T. C. So, R. K. Jain, *Mol. Imaging* **1**, 9 (2002).
19. E. B. Brown *et al.*, *Nature Med.* **7**, 864 (2001).
20. VEGF-C was shown qualitatively to increase the size of peritumor LYVE-1–stained vessels in (*16*).
21. Only three ITLs were found. One ITL per tumor was found in 3 of 14 tumors at depths of 160 μm (MT), 200 μm (VEGF-C), and 260 μm (VEGF-C).
22. M. Jeltsch *et al.*, *Science* **276**, 1423 (1997).
23. E. K. Rofstad *et al.*, *Cancer Res.* **62**, 661 (2002).
24. J. Trzewik, S. K. Mallipattu, G. M. Artmann, F. A. Delano, G. W. Schmid-Schonbein, *FASEB J.* **15**, 1711 (2001).
25. G. Helmlinger, P. A. Netti, H. C. Lichtenbeld, R. J. Melder, R. K. Jain, *Nature Biotechnol.* **15**, 778 (1997).
26. S. J. Mandriota *et al.*, *EMBO J.* **20**, 672 (2001).
27. M. Skobe *et al.*, *Nature Med.* **7**, 192 (2001).
28. T. Karpanen *et al.*, *Cancer Res.* **61**, 1786 (2001).
29. T. Makinen *et al.*, *EMBO J.* **20**, 4762 (2001).
30. R. K. Jain, T. P. Padera, *J. Natl. Cancer Inst.* **94**, 785 (2002).
31. We thank D. Jackson, S. Tomarev, K. Alitalo, B. Seed, P. So, and A. Hartford for reagents and advice; S. Roberge, P. Huang, C. Swandal, D. Capen, and R. Delgiacco for outstanding technical support; and D. Fukumura, B. Fenton, and B. Stoll for discussion. Supported by NIH (Bioengineering Research Partnership Grant R24-CA85140). T.P.P. received an NSF Graduate Fellowship.

Supporting Online Material
www.sciencemag.org/cgi/content/full/1071420/DC1
Materials and Methods
SOM Text
Figs. S1 to S4
Tables S1 and S2

28 February 2002; accepted 29 March 2002
Published online 25 April 2002;
10.1126/science.1071420
Include this information when citing this paper.

Structure of an HIF-1α–pVHL Complex: Hydroxyproline Recognition in Signaling

Jung-Hyun Min,[1] Haifeng Yang,[2] Mircea Ivan,[2] Frank Gertler,[4] William G. Kaelin Jr.,[2,3] Nikola P. Pavletich[1]*

The ubiquitination of the hypoxia-inducible factor (HIF) by the von Hippel–Lindau tumor suppressor (pVHL) plays a central role in the cellular response to changes in oxygen availability. pVHL binds to HIF only when a conserved proline in HIF is hydroxylated, a modification that is oxygen-dependent. The 1.85 angstrom structure of a 20-residue HIF-1α peptide–pVHL–ElonginB–ElonginC complex shows that HIF-1α binds to pVHL in an extended β strand–like conformation. The hydroxyproline inserts into a gap in the pVHL hydrophobic core, at a site that is a hotspot for tumorigenic mutations, with its 4-hydroxyl group recognized by buried serine and histidine residues. Although the β sheet–like interactions contribute to the stability of the complex, the hydroxyproline contacts are central to the strict specificity characteristic of signaling.

The cellular response to oxygen is a central process in animal cells and figures prominently in the pathophysiology of several diseases, including cancer, cardiovascular disease, and stroke (*1*). This process is coordinated by the hypoxia-inducible factor (HIF) and its regulator, the von Hippel–Lindau tumor suppressor protein (pVHL) (*2*, *3*). HIF is a heterodimeric transcription factor that activates the expression of genes involved in angiogenesis, erythropoiesis, energy metabolism, apoptosis, and/or proliferation in response to low-oxygen tension (hypoxia) conditions. pVHL inhibits HIF activity under normal oxygen conditions (normoxia) by targeting the HIF α subunits for polyubiquitination and proteasomal degradation (*4*–*8*). Under hypoxic conditions the HIF α subunits are not recognized by pVHL, and they consequently accumulate and dimerize with HIF-1β (*2*, *3*). *VHL* is mutated in the von Hippel–Lindau cancer predisposition syndrome and in sporadic clear-cell renal carcinomas, and this is associated with constitutively high levels of HIF-1α and the development of highly vascularized tumors (*2*).

pVHL is the substrate-recognition subunit of a ubiquitin-protein ligase that also contains ElonginB, ElonginC, Cul2, and Rbx1 (VBC-CR complex) (*6*–*9*). VBC-CR and the related Skp1–Cul1–F-box (SCF) family of ubiquitin-protein ligases (*10*) catalyze the transfer of ubiquitin from a ubiquitin-conjugating enzyme to specific lysine residues on the substrate (*11*).

pVHL binding to HIF-1α is dependent on the hydroxylation of a core proline residue (Pro^{564}) within the HIF-1α oxygen-dependent degradation domain (ODD) (*12*–*14*). This modification is carried out by recently identified HIF prolyl hydroxylases (HPHs) only in the presence of oxygen (*15*–*17*). A 20-residue HIF-1α ODD region (destruction sequence), conserved in animal orthologs and paralogs, is necessary and sufficient for hydroxylation by HPHs and for binding to pVHL (*12*, *13*).

To investigate the targeting of HIF-1α by the VBC-CR ubiquitin-protein ligase and the basis of hydroxyproline recognition in intracellular signaling, we determined the 1.85 Å crystal structure of the pVHL–ElonginB–ElonginC (VBC) complex bound to the hydroxyproline-containing 20-residue destruction sequence of HIF-1α (Table 1 and fig. S1). The structure shows that a 15–amino acid portion of HIF-1α (residues 561 to 575) adopts an extended, β strand–like conforma-

Table 1. Statistics from the crystallographic analysis. Details of the crystallization and structure determination are provided in the supplementary material (*22*). The statistics for the outermost shell, 1.92 to 1.85 Å, are shown in parentheses. rmsd, Root mean square deviations from ideal geometry and root mean square variation in the *B*-factor of bonded atoms.

Parameter	Data
Beam line	MacCHESS F1
Resolution (Å)	1.85
Observations	248,351
Unique reflections	34,115
Data coverage (%) (last shell, 1.92–1.85)	88.7 (76.5)
R_{sym}* (%) (last shell, 1.92–1.85)	7.9 (38.2)
Refinement statistics (15.0–1.85)	
Reflections ($\|F\| > 0\sigma$)	33,935
Total atoms	3409
Water atoms	523
R-factor† (%) (last shell, 1.92–1.85)	19.6 (24.8)
R_{free}‡ (%) (last shell, 1.92–1.85)	23.6 (29.3)
rmsd bonds (Å)	0.007
rmsd angles (°)	1.40
rmsd *B*-factor (Å^2)	3.7

*$R_{sym} = \Sigma_h\Sigma_i |I_{h,i} - I_h|/\Sigma_h\Sigma_i I_{h,i}$ for the intensity (I) of i observations of reflection h. †R factor $= \Sigma||F_o| - |F_c||/\Sigma|F_o|$, where F_o and F_c are the observed and calculated structure factors, respectively. ‡R_{free} = R factor calculated using 5% of the reflection data chosen randomly and omitted from the start of refinement.

[1]Cellular Biochemistry and Biophysics Program and Howard Hughes Medical Institute, Memorial Sloan-Kettering Cancer Center, New York, NY 10021, USA. [2]Dana-Farber Cancer Institute and [3]Howard Hughes Medical Institute, Harvard Medical School, Boston, MA 02115, USA. [4]Department of Biology, Massachusetts Institute of Technology, Cambridge, MA 02139, USA.

*To whom correspondence should be addressed. E-mail: nikola@xray2.mskcc.org.